Synthesis, spectroscopic characterization, DFT, molecular docking and *in vitro* antibacterial potential of novel quinoline derivatives

Younos Bouzian [a], Yusuf Sert [b,*], Khalid Karrouchi [c,*], Luc Van Meervelt [d], Karim Chkirate [a], Lhassane Mahi [e], Noureddine Hamou Ahabchane [a], Ahmed Talbaoui [f], El Mokhtar Essassi [a]

[a] *Laboratory of Heterocyclic Organic Chemistry, Department of Chemistry, Faculty of Sciences, Mohamed V University, BP1014, Rabat, 10100, Morocco.*

[b] *Sorgun Vocational School, Science and Art Faculty-Department of Physics, Yozgat Bozok University, Yozgat, Turkey.*

[c] *Laboratory of Analytical Chemistry and Bromatology, Faculty of Medicine and Pharmacy, Mohammed V University in Rabat, Morocco.*

[d] *Department of Chemistry, Biochemistry, Molecular and Structural Biology Section, KULeuven, Celestijnenlaan 200F, 3001 Leuven, Belgium*

[e] *Moroccan Foundation for Advanced Science, Innovation and Research (Mascir). Department of Nanotechnology. Rabat Design Center, Rue Mohamed Al Jazouli – Madinat Al Irfane Rabat 10 100, Morocco.*

[f] *Laboratoire de Biologie des Pathologies Humaines, Faculté des Sciences, Université Mohammed V, Rabat, Morocco.*

* Corresponding authors:

Khalid.karrouchi@um5s.net.ma (K. Karrouchi)

yusufsert1984@yahoo.com.tr (Y. Sert)

Abstract

In this work, three new quinolone derivatives were prepared by alkylation of 2-oxo-1,2-dihydroquinoline-4-carboxylic acid with ethyl 2-bromoacetate. The synthesized compounds **2-4** were characterized by using FT-IR, ^{1}H NMR, ^{13}C NMR and mass spectrometry. Crystal structure of **4** was determined by single crystal X-ray diffraction. The optimized structures of **2-4** in gas phase, ^{1}H and ^{13}C NMR chemical shifts, molecular electrostatic potential (MEP), frontier orbitals and non-linear properties (NLO) have been investigated by using the B3LYP/6-311++G(d,p) method. All compounds were evaluated *in vitro* for their antibacterial activities against *Pseudomonas aeruginosa* ATCC 27853, *Escherichia coli* ATCC4157, *Streptococcus faecalis* ATCC 29212 and *Staphylococcus aureus* ATCC 25923 bacterial strains. The tested compounds exhibited a good to moderate antibacterial activity with MIC values between 6.25 and 50 µg/mL, when compared to references Ampicillin and Chloramphenicol. Among the three compounds, compound **4** showed the most potent antibacterial activity against *S. aureus* with MIC value of 6.25 µg/mL. In addition, molecular docking studies of compounds **2-4** were performed within the active site of PDB: 2ZCQ protein to analyze the binding interactions responsible for their activities.

Keywords: Synthesis**,** Quinoline; Crystal structure; DFT; Antibacterial activity; Molecular docking.

1. Introduction

Bacterial infections are one of the most widespread causes of persistent disease and affect millions of people with a higher level of morbidity and mortality [1]. Antibiotics drugs were developed to treat bacterial infections, and resistance to them develops when bacteria progress in response to their presence. Priority antibiotic-resistant pathogens constitute the major risk to human health [2], and antibiotic resistance has become a major focus for researchers. Therefore, there is an urgent need to identify and develop new antibiotic agents that kill resistant bacteria with a new mode of action and broad spectrum activities.

Quinoline derivatives are an important class of heterocyclic compounds that occupy an important place in the design of new compounds bioactive [3-5]. In the search for a new scaffold for antimicrobial drugs, this class of heterocyclic compounds, has shown great potential, as various quinoline analogues, have been reported to possess a wide range of biological activities such as antibacterial [6], antitubercular [7], antimalarial [8], antiviral [9], antileishmanial [10], anticancer [11], anti-inflammatory [12], analgesic [13], anti-Alzheimer [14], cardiovascular [15] and tyrosine kinase inhibition [16]. Also, quinoline ring is present in the structure of several synthetic antibiotic agents such as Ciprofloxacin, Levofloxacin, and Norfloxacin (Fig. 1). Over the past few decades, several attempts have been made to investigate the structure–activity relationship of the antimicrobial activity of this scaffold; for instance, the derivatives of quinoline bearing carbonitrile [17], pyrazoline [18], hydrazone [19], quinazoline and thiazolidine [20] and thiadiazole [21].

Given the therapeutic properties of these derivatives, the determination of the structural, geometrical and electronic properties by using DFT calculations is essential to know the influence of different substituents on the pharmacological properties of these molecules [12-26]. In continuation of our work on the design and synthesis of new heterocyclic compounds with potential biological activity [27-32], in this study, three new quinoline derivatives (**2-4**) have been synthesized by alkylation of 2-oxo-1,2-dihydroquinoline-4-carboxylic acid with ethyl acetate bromide under the conditions of liquid-solid phase transfer catalysis. Molecular structure of the synthesized compounds were characterized by FT-IR, ^{1}H-NMR, ^{13}C-NMR, mass spectrometry and crystal structure of compound **4** was determined by single crystal X-ray diffraction. The optimized molecular structures, ^{1}H and ^{13}C NMR chemical shifts, Molecular Electrostatic Potential (MEP), Frontier Orbitals, and Non-Linear Properties (NLO) of the title molecules have been investigated by using the B3LYP/6-311++G(d,p) method. In addition, Molecular docking studies of the title compounds were performed using the

carotenoid dehydrosqualene synthase from *Staphylococcus aureus* (PDB: 2ZCQ) to investigate the binding interactions at the active sites.

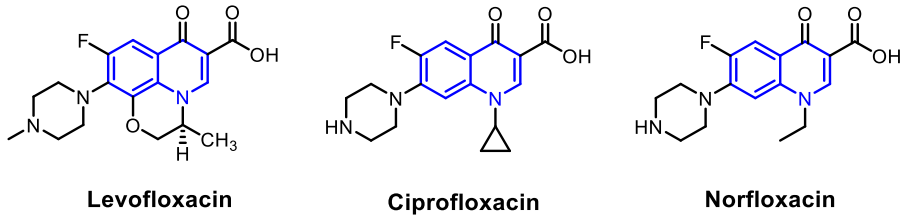

Figure 1. Molecular structures of Ciprofloxacin, Levofloxacin, and Norfloxacin.

2. Experimental

2.1. General methods

Chemical reagents were purchased from Fluka, Sigma and Aldrich chemicals. Reactions were checked with TLC using silica gel 60 F254 from Merck. Melting points were measured using a Buchi B-545 digital capillary melting point apparatus and are uncorrected. The FT-IR spectrum was recorded with Perkin-Elmer VERTEX 70 FT-IR spectrometer over the range 400–4000 cm^{-1}. ^{1}H and ^{13}C NMR spectra were recorded in DMSO-d_6 solutions on a Bruker spectrometer (300 MHz).

General procedure for the synthesis of compounds 2-4

A mixture of 2-oxo-1,2-dihydroquinoline-4-carboxylic acid (1 g, 5.29 mmol), K_2CO_3 (1.61 g (2.92 g for **4**), 11.63 mmol (or 21.16 mmol for **4**)), ethyl bromoacetate (1.46 mL, 13.22 mmol) in DMF (45 mL), tetra *n*-butylammonium bromide was added. The mixture was stirred for 48 h at room temperature. After removal of the salts by filtration, the solvent was evaporated and the residue obtained was purified by column chromatography using silica gel (eluent: hexane/ ethyl acetate) to afford new compounds **2** and **3** or **4** (Scheme 1).

2-ethoxy-2-oxoethyl 1-(2-ethoxy-2-oxoethyl)-2-oxo-1,2-dihydroquinoline-4-carboxylate (2)

Colorless crystals, Yield = 60%, m.p = 105 °C; ^{1}H NMR (300 MHz, DMSO-d_6) δ ppm : 8.15 (dd, ^{3}J = 8.1Hz, ^{4}J = 1.4 Hz, 1H, CHar), 7.75 – 7.63 (m, 1H, CHar), 7.53 (d, ^{3}J = 8.3 Hz, 1H, CHar), 7.36 (m, 1H, CHar), 7.02 (s, 1H, CHar), 5.14 (s, 2H, OCH_2), 5.02 (s, 2H, NCH_2), 4.28 – 4.19 (q, ^{3}J = 6.6 Hz, 2H, OCH_2), 4.19 – 4.11 (q,^{3}J = 6.6 Hz, 2H, NCH2), 1.24 (t, ^{3}J = 5.7 Hz, 3H, CH3), 1.19 (t, ^{3}J = 5.7 Hz, 3H, CH_3); ^{13}C NMR (75 MHz, DMSO-d_6) δ ppm: 168.36 (CO), 167.84, 165.14, 160.43 (CO), 140.27, 140.08, 122.39 (Cq) 132.39, 127.01, 123.37,

122.55, 115.78 (CHar), 62.56, 61.74 (OCH_2), 44.41 (NCH_2), 14.48 (CH_3); ESI-MS: m/z = 362.1240 $[M-H]^+$.

2-ethoxy-2-oxoethyl 2-(2-ethoxy-2-oxoethoxy) quinoline-4-carboxylate (3)

Colorless crystals, Yield = 20%, m.p = 58 °C; ^{1}H NMR (300 MHz, DMSO-d_6) δppm : 8.46 (d, ^3J = 8.3 Hz, 1H, CHar), 7.84 – 7.70 (m, 1H, CHar), 7.57 (m, 1H, CHar), 7.51 (s, 1H, CH), 5.07 (s, 2H, OCH_2), 5.05 (s, 2H, OCH_2), 4.26 – 4.18 (q,^3J = 6.6 Hz, 2H, OCH_2), 4.18 – 4.11 (q,^3J = 6.6 Hz, 2H, OCH_2), 1.23 (t, ^3J = 7.1 Hz, 3H, CH_3), 1.17 (t, ^3J = 7.1 Hz, 3H, CH_3); ^{13}C NMR (75 MHz, DMSO-d_6) δ ppm: 168.86 (CO), 167.90, 165.24, 160.15(CO), 146.65, 139.04, 121.68 (Cq), 131.28, 127.91, 126.40, 125.63, 114.35(CHar), 63.16, 62.51, 61.69, 61.03(OCH_2), 14.51, 14.47(CH_3); ESI-MS: m/z = 362.1240 $[M-H]^+$.

Ethyl 1-(2-ethoxy-2-oxoethyl)-2-oxo-1,2-dihydroquinoline-4-carboxylate (4)

Colorless crystals, Yield = 50%, m.p = 112 °C; ^{1}H NMR (300 MHz, $CDCl_3$) δ ppm: 8.38 (dd, ^3J = 8.2Hz,^4J = 1.3 Hz, 1H, CHar), 7.60 (m, 1H, CHar), 7.36 – 7.27 (m, 1H, CHar), 7.24 (s, 1H, CHar), 7.16 (d, ^3J = 8.5 Hz, 1H, CHar), 5.13 (s, 2H, OCH_2), 4.48 (q, ^3J = 7.1 Hz, 2H, OCH_2), 4.26 (q, J = 7.1 Hz, 2H, NCH_2), 1.45 (t, ^3J = 7.1 Hz, 3H, CH_3), 1.28 (t, ^3J = 7.1 Hz, 3H, CH_3). ^{13}C NMR (75 MHz, $CDCl_3$) δ ppm: 167.73 (CO), 165.23, 161.12 (C=O), 139.78, 139.66, 117.63 (Cq) 131.38, 127.55, 123.71, 123.04, 113.95 (CHar), 62.16, 61.92 (OCH_2), 44.04 (NCH_2), 14.17, 14.13 (CH_3); EI-MS: m/z = 303.1636 $[M]^+$.

2.2. Computational details

In this research article, all quantum chemical computations (optimizations, NMR, frontier orbitals, molecular electrostatic potentials, non-linear properties) were carried out by using density functional theory (DFT) method with Becke's three-parameter hybrid exchange functional and the Lee-Yang-Parr [33] correlation functional at B3LYP/6-311++G(d,p) level of theory included within the Gaussian 09 package [34]. Gauss view 5.0 interface program [35] was used to prepare input to Gaussian and to examine graphically the output that Gaussian calculates. The initial coordinates for the molecular optimization and other computations in compound **3** [36] and **4** were utilized from CIF (crystal information file) files. But, the initial coordinates for compound **2** (there is no CIF file) were prepared with the help of Gauss view 5.0. Hirshfeld surface analysis of compound **3** and **4** was performed by using Crystal Explorer 3.1 program [37]. Finally, the molecular docking investigations were performed by using AutoDock Vina free software program [38].

2.3. X-ray analysis

A single crystal of **4** was obtained by X-ray intensity data were collected at 293(2) K on an Agilent SuperNova diffractometer with Eos CCD detector using MoKα radiation. The images were processed (unit cell determination, intensity data integration, correction for Lorentz and polarization effects, and empirical absorption correction) using CrysAlisPRO [39]. Using Olex2 [40], the structure was solved with the ShelXT [41] structure solution program using Intrinsic Phasing and refined with the ShelXL [42] refinement package using full-matrix least-squares minimization on F^2. All H atoms were placed in idealized positions and refined in the riding mode. Non-hydrogen atoms were refined anisotropically and hydrogen atoms in the riding mode with isotropic temperature factors fixed at 1.2 times U_{eq} of the parent atoms (1.5 times U_{eq} for CH_3). One of the ethyl groups was found to be disordered over two orientations with occupancies 0.853(19) and 0.147(19). At the end of the refinement the R_1-value converged to 0.0560. Crystal data, data collection and structure refinement details are summarized in Table 1.

2.4. Antibacterial activity

The antibacterial activity of the synthesized compounds was determined according to the method described in our previous work [43].

3. Results and discussion

3.1. Chemistry

The alkylation reaction of 2-oxo-1,2-dihydroquinoline-4-carboxylic acid (**1**) with ethyl acetate bromide under the conditions of liquid-solid phase transfer catalysis in DMF, in the presence of 2.2 equivalents of potassium carbonate (K_2CO_3) as base, and tetra n-butylammonium bromide (BTBA) as catalyst, leads to the two products **2** and **3**, with a yield of 80%. On the other hand, under the same conditions but in the presence of four equivalents of potassium carbonate (K_2CO_3), a new compound **4** is obtained with a yield of 50% with the formation of compounds **2** and **3** in small quantities. These results show that the amount of potassium carbonate has an influence on the alkylation reaction of 2-oxo-1,2-dihydroquinoline-4-carboxylic acid **1**. Ethyl bromide acetate reacts as an alkylating agent of compound **1**, leading to di-alkylated quinoline **2**.

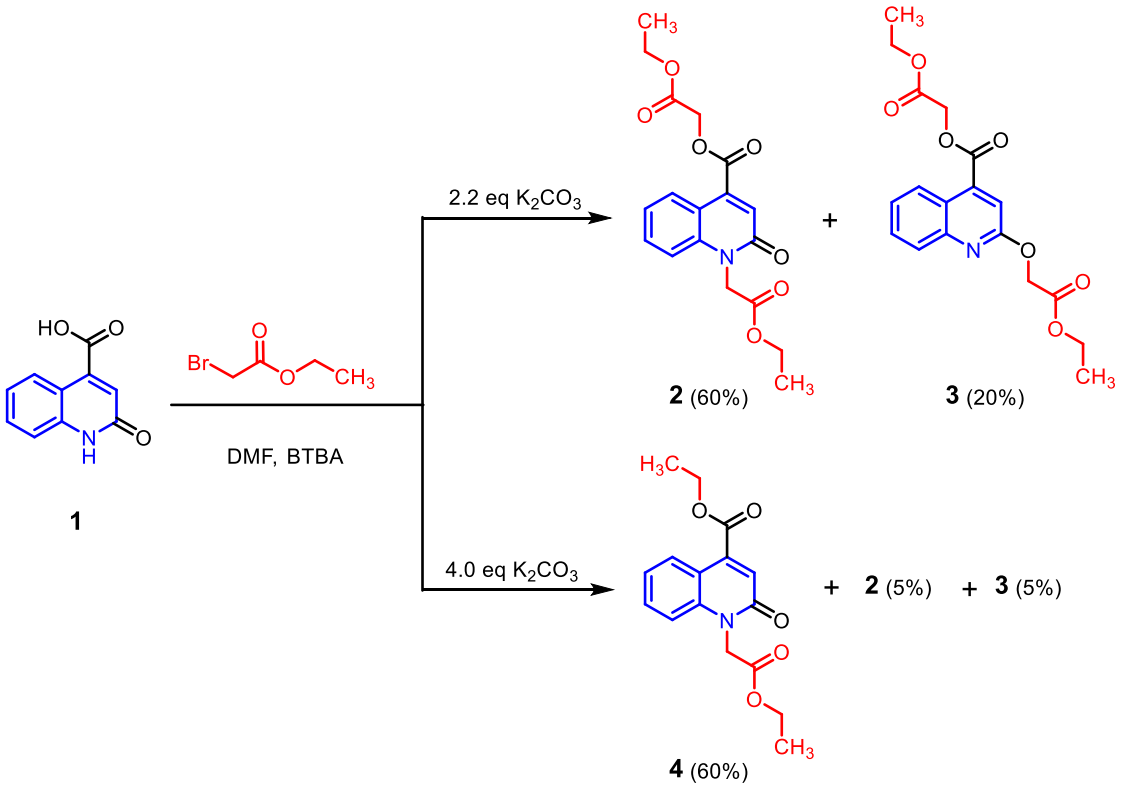

Scheme 1. Synthetic route for preparation of compounds **2-4.**

Under the reaction conditions, ethyl acetate bromide can undergo a hydrolysis reaction to give bromoacetic acid (pKa = 2.69) which is strongly acidic, much more acidic than acetic acid (pKa = 4.76) and ethanol. In a transesterification reaction, to form the ester **4**, one can start from an ester in position 4 of the di-alkylated quinoline **2** and add ethanol to it (Fig. 2). The reaction is catalyzed in an acidic or basic medium.

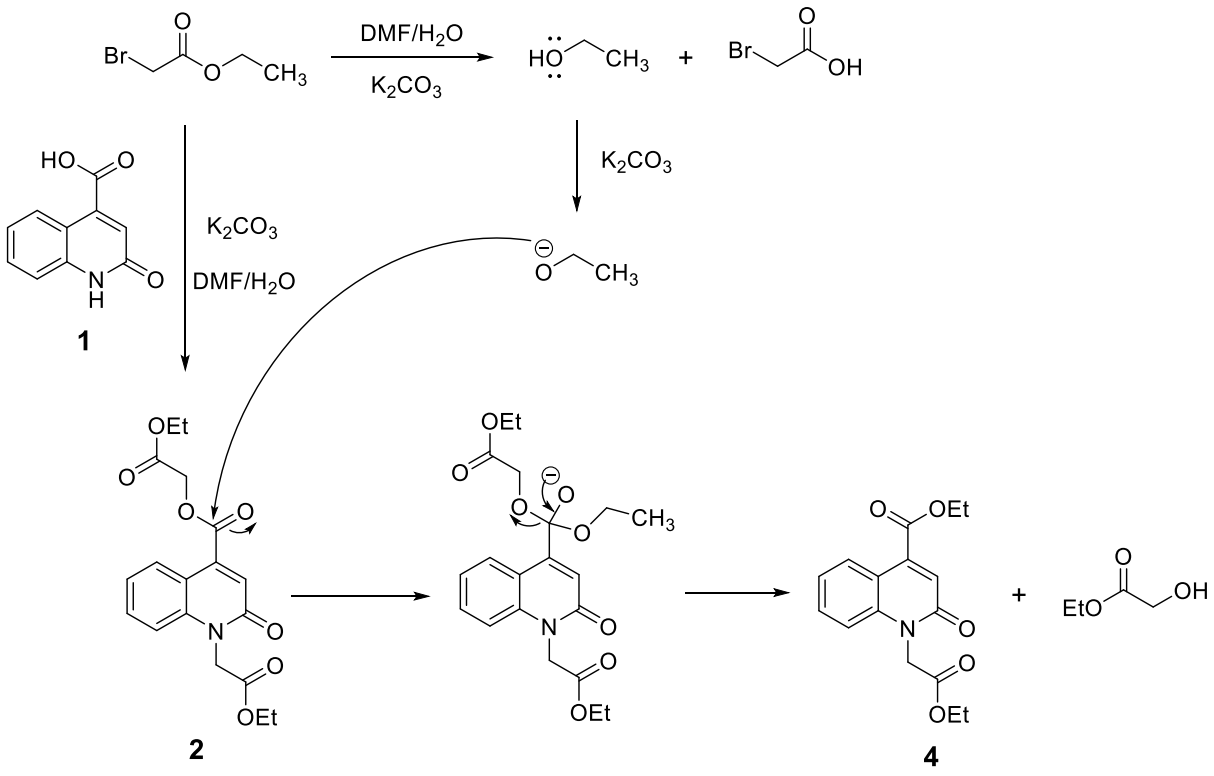

Figure 2. Plausible reaction mechanism for the formation of **4**.

3.2. X-ray structure description and optimized geometry

Crystals of **4** belong to the monoclinic space group $P2_1/c$. The asymmetric unit is illustrated in Fig. 3. The terminal methyl group C22 is disordered over two orientations (C22A and C22B) in a 0.853(19):0.147(19) ratio. The quinoline ring is planar (r.m.s. deviation 0.046 Å) with atoms C11, O17 and C18 close to this plane (deviations of 0.272(3), -0.137(3) and 0.196(3) Å, respectively). The crystal packing of **4** is characterized by C-H…O and C-H…π interactions (Fig. 4). Geometrical details of the C9-H9…O17 interaction are: C9-H9 = 0.93 Å, H9…O17^{ii} = 2.42 Å, C9…O17^{ii} = 3.229(3) Å, C9-H9…O17^{ii} = 145° [symmetry code: (ii) 1 – *x*, 1/2 + *y*, 3/2 - *z*]. Additional C-H…O interactions C8-H8…O19, C11-H11…O13 and C21-H21A…O19 are much weaker and not shown in Fig. 4. Geometrical details of the C15-H15A…π(C5–C10) interaction are: C15-H15A = 0.97 Å, H15A…*Cg*2^{i} = 2.80 Å, C15… *Cg*2^{i} = 3.598(3) Å, C15-H15A…*Cg*2^{i} = 141° [*Cg*2 is the centroid of ring C5-C10; symmetry code: (i) 1 – *x*, -1/2 + *y*, 3/2 - *z*].

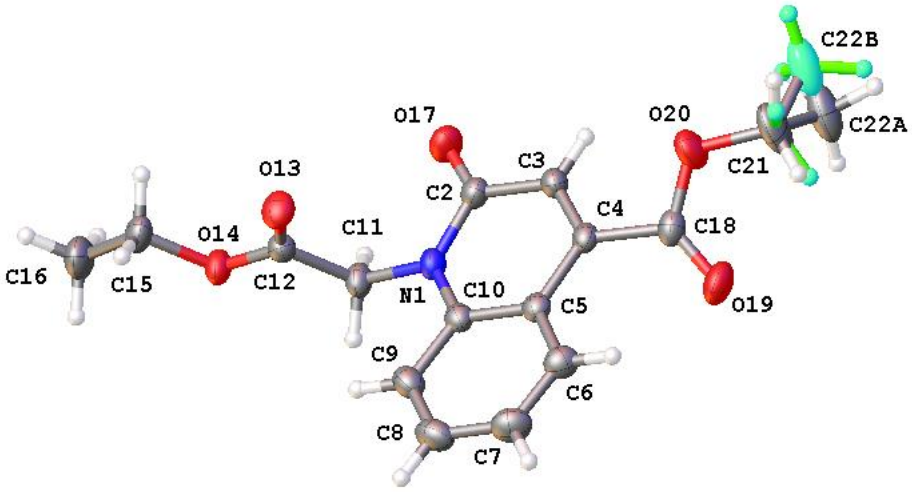

Figure 3. The molecular structure of **4** showing 30% displacement ellipsoids.

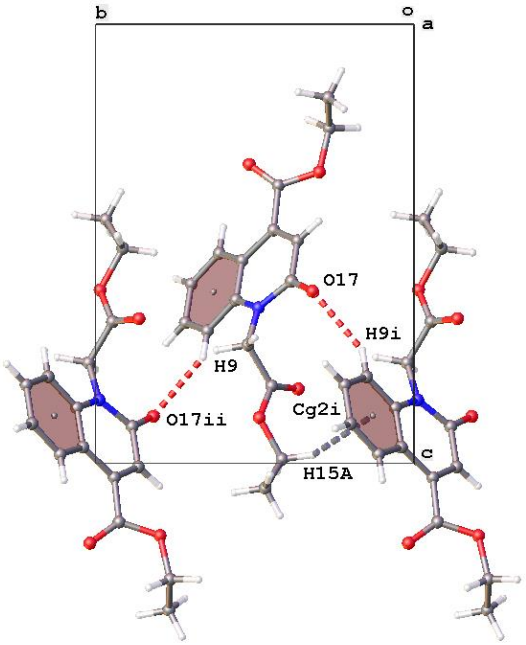

Figure 4. Partial crystal packing of **4** showing the C-H…O (red dashed line) and C-H…π (grey dashed line) interactions [*Cg*2 is the centroid of ring C5-C10; symmetry codes: (i) 1 – *x*, -1/2 + *y*, 3/2 - *z*; (ii) 1 – *x*, 1/2 + *y*, 3/2 - *z*].

Table 1. Crystallographic and refinement data for **4.**

CCDC Deposition Number	CCDC 2064962
Chemical formula	$C_{16}H_{17}NO_5$
M_r	303.30
Crystal system, space group	Monoclinic, $P2_1/c$
Temperature (K)	293
a, b, c (Å)	11.4774 (5), 9.7985 (3), 14.0539 (6)
β (°)	106.022 (4)
V (Å^3)	1519.13 (11)
Z	4
Radiation type	Mo $K\alpha$
μ (mm^{-1})	0.10
Crystal size (mm)	0.35 × 0.3 × 0.2
Data collection	
Diffractometer	SuperNova, Single source at offset/far, Eos
Absorption correction	Multi-scan *CrysAlis* PRO
T_{min}, T_{max}	0.777, 1.000
No. of measured, independent and observed [$I > 2\sigma(I)$] reflections	11213, 3107, 2163
R_{int}	0.027
$(\sin \theta/\lambda)_{max}$ (Å^{-1})	0.625
Refinement	
$R[F^2 > 2\sigma(F^2)]$, $wR(F^2)$, S	0.056, 0.154, 1.05
No. of reflections	3107
No. of parameters	207
No. of restraints	2
H-atom treatment	H-atom parameters constrained
$\Delta\rho_{max}$, $\Delta\rho_{min}$ (e Å^{-3})	0.45, −0.29

The optimized structure parameters of compound **2** (2-ethoxy-2-oxoethyl 1-(2-ethoxy-2-oxoethyl)-2-oxo-1,2-dihydroquinoline-4-carboxylate), compound **3** (2-ethoxy-2-oxoethyl 2-(2-ethoxy-2-oxoethoxy) quinoline-4-carboxylate) and compound **4** (ethyl 1-(2-ethoxy-2-oxoethyl)-2-oxo-1,2-dihydroquinoline-4-carboxylate) were calculated with the help of DFT/B3LYP method and 6-311++G(d,p) basis set. As mentioned before, for initial coordinates CIF files were used except for compound **2**. The obtained results were given comparatively as in Table S1 and the optimized structures are shown in Fig. 5**.** There are some differences between experimental and computed results due to the phase difference (experimental results in solid and theoretical ones in gas phase). Despite this, fairly consistent results were obtained.

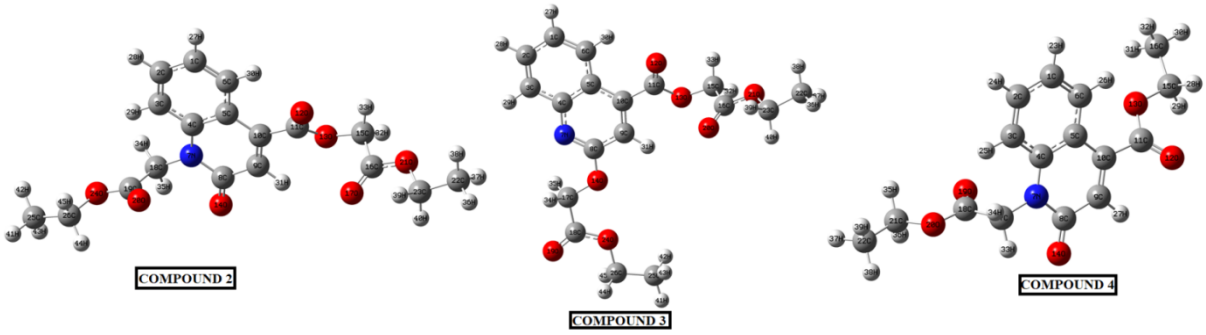

Figure 5. The optimized structures of title compounds.

3.3. FT-IR study

The experimental FT-IR spectra of compounds **2-4** in the solid state are given in Figs. S1-S3. The C-H stretching vibrations of aromatic rings give rise to bands in the region 3200–3000 cm^{-1} in aromatic compounds [24, 25]. For the title compounds, a series of infrared bands in the range 3078-3014 cm^{-1} were assigned as CH (sp^2 and sp^3) stretching modes. On the other hand, the CH_3 and CH_2 antisymmetric and symmetric vibration modes were observed between 2992 and 2852 cm^{-1}. The C=O vibration mode is generally one of the most intense peak in an infrared spectrum; it appears in a region 1800–1600 cm^{-1} [24,25]. Here, the C=O stretching mode in the title compounds is assigned to the intense band at 1754, 1739, 1728 and 1655 cm^{-1} for **2**, at 1740, 1723 and 1600 cm^{-1} for **3** and at 1740, 1717 and 1655 cm^{-1} for **4**. The C=N stretching vibrations in compound **3** is observed at 1572 cm^{-1}. The aromatic C=C stretching vibrations of pyridyl and phenyl rings are very much important and occur in the region 1200-1650 cm^{-1}. For the studied compounds, a series of infrared bands having significant νC=C contributions were observed bands between 1608 and 1439 cm^{-1}.

3.4. NMR studies

The experimental ^{1}H- and ^{13}C-NMR spectra of compounds **2-4** were recorded in DMSO-d_6 or $CDCl_3$ as solvent (Figs. S4-S9). The experimental chemical shifts of protons and C atoms compared with the corresponding predicted by using B3LYP/6-311++G(d,p) level by using IEFPCM model and GIAO method with the hybrid B3LYP/6-311++G** method are summarized in Table 2**.** The ^{1}H NMR spectra of compounds **2** and **3** shows the insertion of the ethoxycarbonyl ethyl group in compound **1**, attested by the disappearance of NH and OH signals and the appearance of two singlets at 1.19 and 1.24 ppm for **2** (1.17 and 1.24 ppm for **3**) relative to two methyl (CH_3) protons of ethyl ester group and four signals at 4.11-4.19, 4.20-4.28, 5.02 and 5.14 ppm for **2** (4.11-4.18, 4.19-4.26, 5.05 and 5.07 ppm for **3**) relative to

methylene (CH_2) protons of ethoxycarbonyl ethyl group. On the other hand, the ^1H NMR spectrum of compound **4**, shows the presence of two singlets at 1.45 and 1.28 ppm due to methyl (CH3) protons and three signals at 4.26, 4.48 and 5.13 ppm due to the methylene (CH_2) protons.

The ^{13}C NMR spectra of compounds **2** and **3** show, in particular, the signals relative to the carbons of the alkyl groups of both isomers, signals are observed at 14.48, 44.41, 61.74 and 62.56 ppm for **2**, and at 14.47, 14.51, 61.03, 61.69, 62.51 and 63.03 ppm for **3** corresponding to the methyl (CH_3) and methylene (CH_2) carbons ethoxycarbonyl ethyl group. The ^{13}C NMR spectrum of compound **4** shows the signals at 14.13, 14.17, 44.04; 61.92 and 62.16 ppm due to the methyl (CH_3) and methylene (CH_2) carbons ethoxycarbonyl ethyl group.

The experimental and calculated NMR shifts were given in Table 2 and the experimental and calculated values are in a very good agreement with each other.

Table 2. The experimental and computed 1H & ^{13}C NMR chemical shifts of compounds **2-4**.

Compound **2**			Compound **3**			Compound **4**		
Atom	δexp.	δcalc.	Atom	δexp.	δcalc.	Atom	δexp.	δcalc.
C1	122.55	129.76	C1	127.91	132.95	C1	123.04	128.75
C2	132.39	139.90	C2	139.28	138.31	C2	127.55	139.43
C3	115.78	120.80	C3	125.63	135.54	C3	113.95	120.05
C4	140.08	149.36	C4	146.65	156.35	C4	139.66	149.74
C5	123.37	125.42	C5	121.68	130.15	C5	123.71	125.19
C6	116.58	135.34	C6	126.40	133.18	C6	117.63	135.57
C8	160.43	169.38	C8	160.15	168.18	C8	161.12	168.54
C9	127.01	131.32	C9	114.35	122.48	C9	131.38	130.12
C10	140.27	148.53	C10	139.04	146.77	C10	139.78	152.69
C11	167.84	175.54	C11	165.24	175.45	C11	167.73	176.87
C15	61.74	67.38	C15	62.51	67.20	C15	62.16	70.05
C16	168.38	178.31	C16	167.90	178.45	C16	14.13	16.34
C18	44.41	48.22	C17	63.16	70.00	C17	44.04	47.65
C19	165.14	179.04	C18	168.86	178.95	C18	165.23	178.22
C22	14.48	16.03	C22	14.47	16.07	C21	61.91	69.43
C23	61.74	69.88	C23	61.06	69.80	C22	14.17	16.22
C25	14.48	16.07	C25	14.51	16.20			
C26	62.56	70.08	C26	61.69	69.66			
Compound **2**			Compound **3**			Compound **4**		
Atom	δexp.	δcalc.	Atom	δexp.	δcalc.	Atom	δexp.	δcalc.
H27	7.36	7.62	H27	7.77	7.89	H23	7.31	7.51
H28	7.68	7.96	H28	7.77	8.14	H24	7.60	7.88
H29	7.52	7.51	H29	8.45	8.27	H25	7.16	7.36
H30	8.15	8.60	H30	7.56	8.99	H26	8.38	8.41
H31	7.02	7.53	H31	7.51	8.01	H27	7.24	7.10
H32	5.14	4.80	H32	5.07	4.83	H28	4.26	4.60
H33	5.14	5.47	H33	5.07	5.51	H29	4.26	4.47
H34	4.15	4.56	H34	5.05	5.14	H30	1.28	1.42
H35	4.15	5.98	H35	5.05	5.08	H31	1.28	1.58
H36	1.24	1.40	H36	1.23	1.40	H32	1.28	1.67
H37	1.24	1.53	H37	1.23	1.54	H33	5.13	6.12
H38	1.24	1.55	H38	1.23	1.57	H34	5?13	4.37

H39	4.23	4.38	H39	4.22	4.38	H35	4.48	4.33
H40	4.23	4.33	H40	4.22	4.39	H36	4.48	4.28
H41	1.19	1.39	H41	1.17	1.47	H37	1.45	1.35
H42	1.19	1.58	H42	1.17	1.69	H38	1.45	1.56
H43	1.19	1.56	H43	1.17	1.69	H39	1.45	1.54
H44	5.02	4.33	H44	4.14	4.43			
H45	5.02	4.38	H45	4.14	4.39			

3.5. Hirshfeld Surface Analysis

In this section, Hirshfeld surface analysis of compounds **3** and **4** were done by Crystal Explorer 3.1 program [31] with the help of CIF files (there is no CIF for compound **2**). For Hirshfeld surface analysis a general formalism can be given as follows:

$$d_{norm} = \frac{d_i - r_i^{VDW}}{r_i^{VDW}} + \frac{d_e - r_e^{VDW}}{r_e^{VDW}} \quad (1)$$

Here, distance from the surface of the Hirshfeld to the nearest core outside the surface is presented as d_e, the distance corresponding to the nearest core in the surface is presented as d_i. d_{norm} value is dependent on d_e, d_i and Van der Waals radius, additionally the r_i^{VDW} and r_e^{VDW} are the Van der Waals radii of the atoms [44-48]. In this equation, d_{norm} values were coded with three different colors such as red, green and blue [49]. In our study, d_{norm} range of -0.2122 to 1.7249 Å for compound **3** and d_{norm} range of -0.2317 to 1.5516 Å for compound **4**. The 3D Hirshfeld surfaces and 2D fingerprint diagrams of compounds **3** and **4** are shown in Fig. 6. Although only one O-H points are given on Figs. 6 and 7, other O-H points can be seen easily. As seen from the Figs. 6 and 7, the most concentrated red points were observed over the O-H bindings, and the occurred possible hydrogen bonding values in crystal structure were determined 2.539 Å and 2.297 Å for compound 3 and 4, respectively.

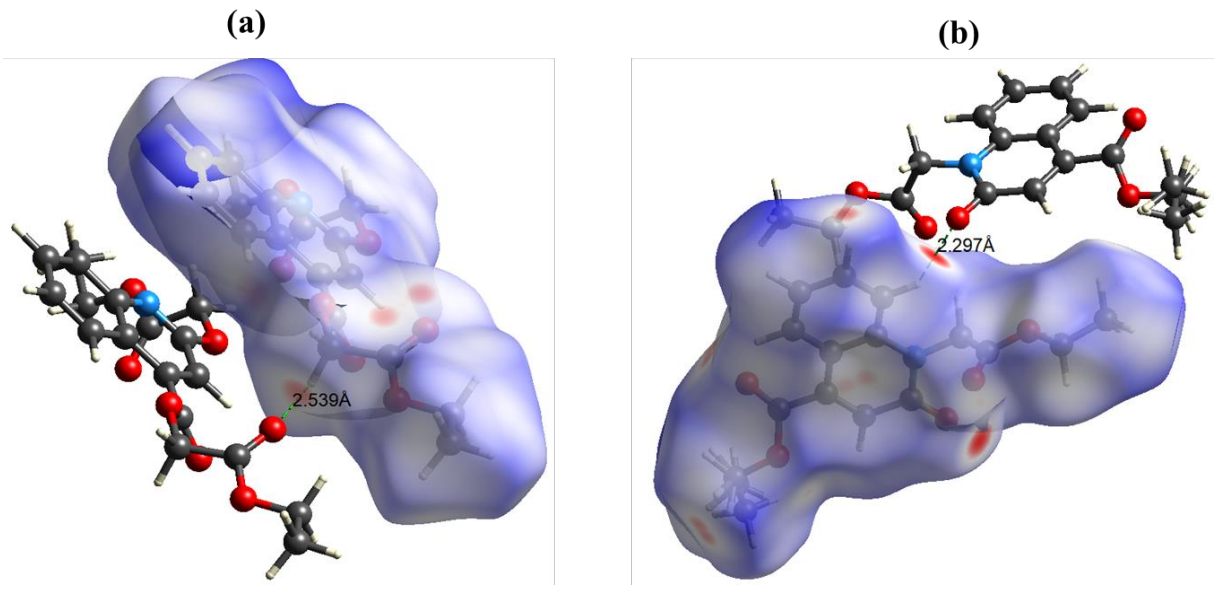

Figure 6. The 3D Hirshfeld surface of **3** (a) and **4** (b).

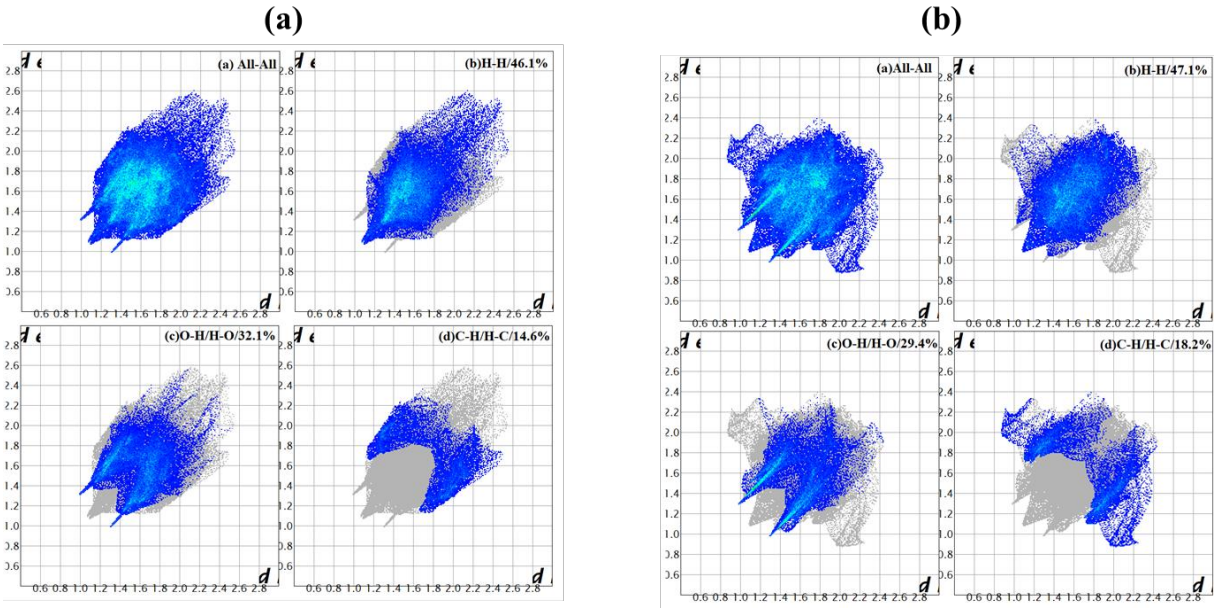

Figure 7. The 2D fingerprint histogram of compounds **3** (a) and **4** (b).

Later, the 2D fingerprint diagrams of compounds **3** and **4** as possible contributions were indicated as in Figure 6 and 7.

3.6. HOMO-LUMO Analysis

The frontier orbitals are known as the highest occupied molecular orbital (HOMO) and the lowest unoccupied molecular orbital (LUMO) and these factors are very important for any organic structure for chemical reactivity. While the HOMO orbital tends to give off electrons,

LUMO tends to acquire electrons. HOMO energy is related to ionization potential while LUMO energy is related to electron activity. In this part, the HOMO-LUMO distributions, their energies in eV unit, and their related quantum chemical descriptors of compounds **2-4** were computed by using DFT/B3LYP method with 6-311++G(d,p) basis set. The calculated parameters (HOMO-LUMO energies, band gap energies, ionization potentials, electron affinities, chemical hardnesses, softnesesses and potentials, electronegativities, electrophilicity indexes and maximum charge transfer indexes) were listed as in Table 3.

Table 3. Some global reactivity descriptors the computed for the title compounds.

Parameters (eV)	Compound **2**	Compound **3**	Compound **4**
E_{LUMO}	-2.351	-2.287	-2.270
E_{HOMO}	-6.375	-6.548	-6.431
Energy bandgap $\lvert E_{HOMO}\text{-}E_{LUMO}\rvert$	4.024	4.260	4.161
Ionization potential ($I = -E_{HOMO}$)	6.375	6.548	6.431
Electron affinity ($A = -E_{LUMO}$)	2.351	2.287	2.270
Chemical hardness ($\eta = (I\text{-}A)/2$)	2.012	2.130	2.081
Chemical softness ($\zeta = 1/2\eta$)	0.249	0.235	0.240
Electronegativity ($\chi = (I+A)/2$)	4.363	4.417	4.351
Chemical potential ($\mu = -(I+A)/2$)	-4.363	-4.417	-4.351
Electrophilicity index ($w = \mu^2/2\eta$)	4.731	4.581	4.549
Maximum charge transfer index ($\Delta N_{max.} = -\mu/\eta$)	2.169	2.074	2.091

The energy difference between HOMO and LUMO is called energy band gap and it is also important in terms of reactivity. From the Table 3, compound **2** is more reactive (Energy bandgap $\lvert E_{HOMO}\text{-}E_{LUMO}\rvert$=4.024 eV) than compounds **3** and **4** according to the energy bandgap=$\lvert E_{HOMO}\text{-}E_{LUMO}\rvert$ values. Additionally, the 3D HOMO and LUMO distributions of compounds **2-4** were shown as in Fig. 8. From the Fig. 8, the HOMO and LUMO distributions were focused on the dihydroquinoline-carboxylate groups for all structures.

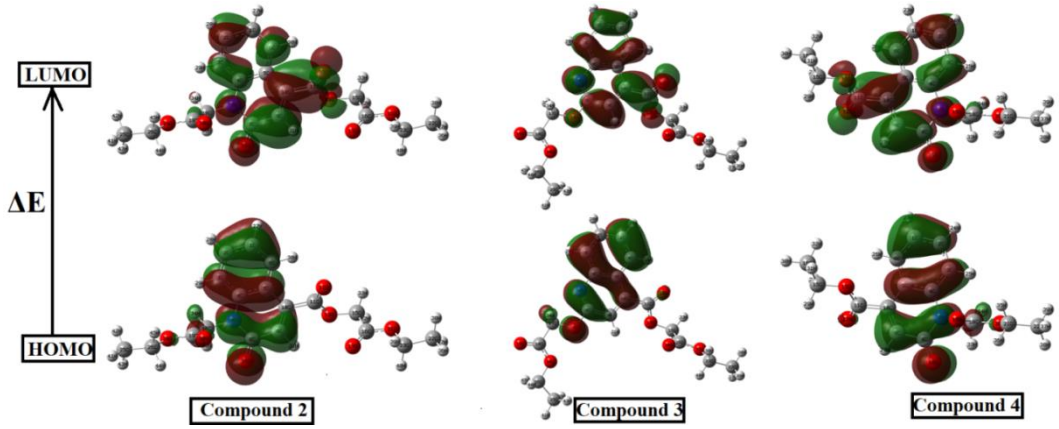

Figure 8. The HOMO and LUMO orbitals of compound **2-4**.

3.7. Molecular Electrostatic Potential Analysis

The molecular electrostatic potential (MEP) analysis is very significant to estimate the reactive sites of the compounds electrophilic and nucleophilic attack [50]. In this part, using the DFT/B3LY method and 6-311++G(d,p) basis set, the molecular electrostatic potential surfaces of the compounds **2-4** were drawn with the shape, size and electrostatic potential values of the molecules and three dimensional potential maps of the iso-electron density surface of the molecules. The obtained MEP contours were indicated as in Fig. 9**.** From the figure, there are three type colors on the MEP which are red, blue and green. Here red represents maximum negative which suitable points for electrophilic attack, blue color indicates the maximum positive which suitable locals for nucleophilic attack points and green color indicates zero value in terms of electron density. Electron-receiving regions shift towards red. It is from the Fig. 9, area having the negative potentials are over electronegative atom (O- dihydroquinoline-4-carboxylate) for three sturctures and having positive potentials are focused over hydrogen atoms. Additionally, the MEP scale was changed from -5.982e-2 to 5.982, -5.015e-2 to 5.015e-2 and -5.938e-2 to 5.938e-2 for compounds **2, 3** and **4**, respectively.

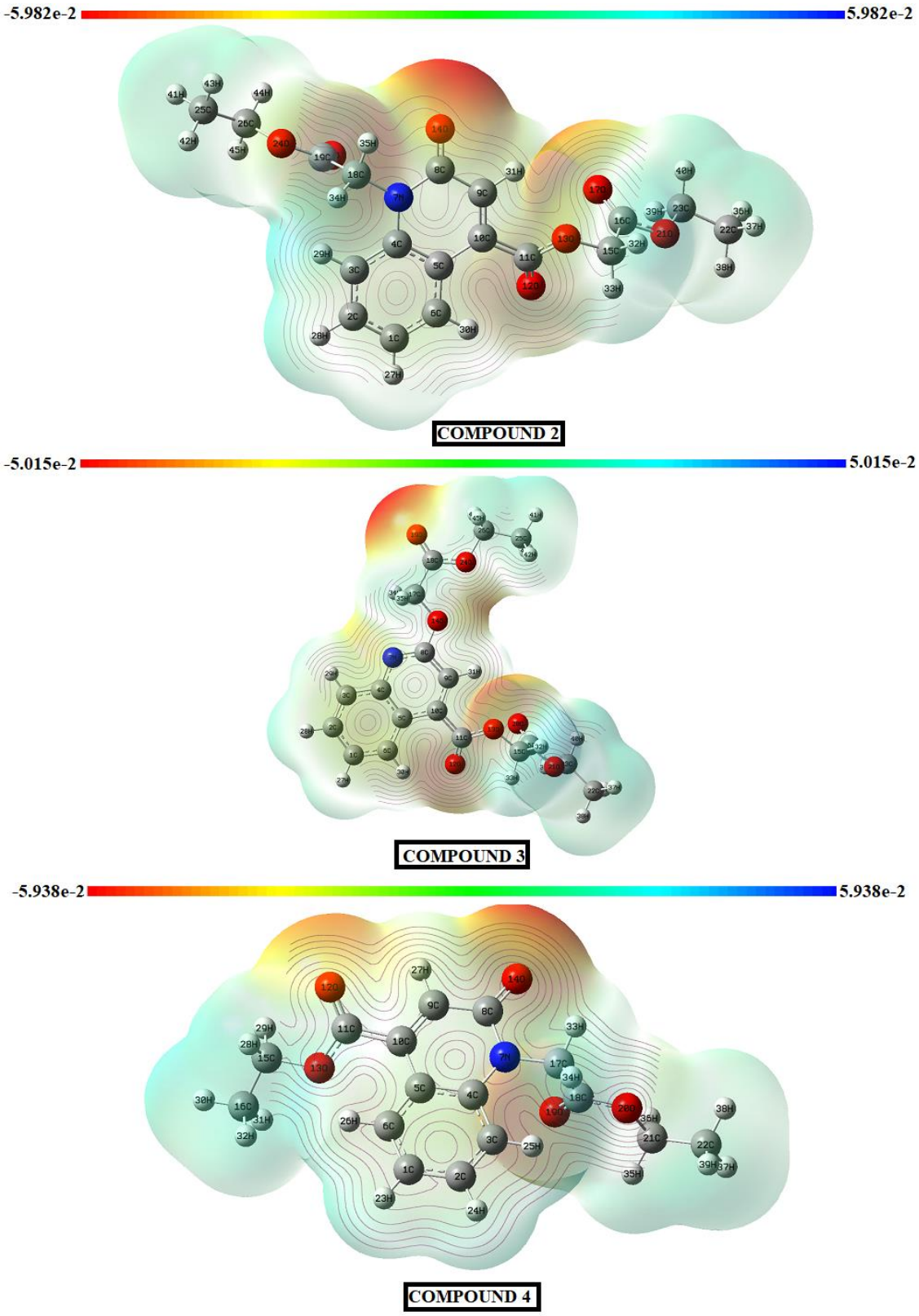

Figure 9. The MEP surfaces of compound **2-4**.

3.8. Non-Linear Properties (NLO)

The NLO analysis is very important for organic compounds. Because they have more advantages over inorganic materials because they show a better NLO response as a result of high polarization effects when interacting with light. NLO analyzes of compounds **2-4** were performed within the scope of the study and the obtained outcomes in terms of components and sizes were listed as in Table S2.

In this part, the mean polarizability(α_{total}) and its components, the anisotropy of polarizability ($\Delta\alpha$), the first order hyper polarizability (β_0) and its components and dipole moments of compounds **2-4** were calculated by B3LYP/6-311++G(d,p) basis set. Urea is taken into account as a general reference due to its properties in the study of nonlinear optical properties. According to this, NLO parameters of urea molecule (α_{total}, $\Delta\alpha$ and β_0) was reported as 5.07643717×10^{-24} esu, 2.13568262×10^{-24} esu and $7.2228469891\times10^{-31}$ esu, respectively. For our computations, the used equations are follows:

$$\alpha_{total} = \frac{1}{3}\left(\alpha_{xx} + \alpha_{yy} + \alpha_{zz}\right) \quad (1)$$

$$\Delta\alpha = \frac{1}{\sqrt{2}}\left[(\alpha_{xx} - \alpha_{yy})^2 + (\alpha_{yy} - \alpha_{zz})^2 + (\alpha_{zz} - \alpha_{xx})^2 + 6a_{xz}^2 + 6a_{xy}^2 + 6a_{yz}^2\right]^{1/2} \quad (2)$$

$$\beta_0 = \left[(\beta_{xxx} + \beta_{xyy} + \beta_{xzz})^2 + (\beta_{yyy} + \beta_{yzz} + \beta_{yxx})^2 + (\beta_{zzz} + \beta_{zxx} + \beta_{zyy})^2\right]^{1/2} \quad (3)$$

$$\mu_{total} = (\mu_x^2 + \mu_y^2 + \mu_z^2)^{1/2} \quad (4)$$

According to the results, the first order hyperpolarizabilities were obtained as 34.704201665 10^{-31}esu, and 48.54607539610^{-31}esu and 30.86761488510^{-31}esu for compound **2, 3** and **4**, respectively, which are 4.81, 6.72 and 4.27 times higher than reference material. Accordingly, it is predicted that the synthesized compounds **2-4** within the scope of the research may be candidates for good NLO properties. Similarly, when we consider α_{total} and $\Delta\alpha$ parameters, it is possible to see similar results as seen from Table 4.

Table 4. The obtained αtotal, Δα and β0 parameters for compounds how many times greater than the reference material urea.

Values	Compound **2**	Compound **3**	Compound **4**
α_{total}	7.29	7.40	6.37
$\Delta\alpha$	9.18	10.24	8.03
β_0	4.81	6.72	4.27

3.9. Antibacterial activity

The newly synthesized compounds **2-4** were evaluated for their antibacterial activities against *E. coli*, *P. aeruginosa*, *S. aureus* and *Streptococcus faecalis* microorganisms by the diffusion method disk [43]. The minimum inhibitory concentration (MIC) is the lowest concentration of samples, for which no growth was detected for 24h at 37°C. The obtained results were compared with Chloramphenicol and Ampicillin as standards. A comparative study of the MIC values of the compounds tested indicates that compound **4** has better activities against the four studied strains. As shown in Table 5, it is evident that compound **4** has an exceptional effect against *S. aureus* with a MIC value of 6.25 µg/ml, this value is 2-fold lower than that of chloramphenicol and ampicillin. Thus, Compound **4** showed good antibacterial activity against *S. faecalis* and *E. coli* with MIC values of 12.5 µg/ml, which is comparable to chloramphenicol and Ampicillin. Compound **2** has a strong activity against *P. aeruginosa* with a MIC value of 12.5 µg/ml, even better than the effect of Ampicillin (MIC =25 µg/ml). Compound **3** has moderate activity against *E. coli*, *P. aeruginosa*, *S. aureus* and *S. faecalis* with a MIC value of 50 µg/ml. Replacing the ethylacetatyl group (compound **2**) with the ethyl group (compound **4**) of the ester function at position 4 of the quinoline ring led to a dramatic improvement in inhibitory activity (MIC = 6.25 µg/mL). This result suggests that an optimal size of the alkyl side chain is required, presumably to fit into the hydrophobic pockets of microbial enzymes, as previously demonstrated by Bhakta et al., [51].

Table 5. MIC of synthesized compounds against growth of bacteria (µg.mL^{-1})**.**

Compounds	*E. coli*	*P. aeruginosa*	*S. aureus*	*S. faecalis*
2	25	**12.5**	50	50
3	50	50	50	50
4	**12.5**	25	**6.25**	**12.5**
Chloramphenicol	6.25	6.25	12.5	12.5
Ampicilline	12.5	25	12.5	6.25

3.10. Molecular Docking Study

Dehydrosqualene synthase (CrtM) from *Staphylococcus aureus* is involved in the synthesis of the carotenoid gold pigment staphyloxanthin [52]. Recent studies have shown that inhibition of *S. aureus* dehydrosqualene synthase reduced bacterial survival during infections, which is a principle of evidence for such a virulence-focused approach [53, 54]. In light of the above facts, molecular docking studies have been conducted to explore the binding interactions between the synthesized compounds **2-4** and the active site of Staphylococcus aureus dehydrosqualene synthase (PDB ID: 2ZCQ). Molecular docking of compounds **2-4** was

performed with the AutoDock Vina program [37] and 3D-PDB format of receptor were downloaded from online protein data bank [55]. The heteroatoms in target were removed and polar hydrogens were added. Later, PDB formats of compound **2-4** were used over the their optimized structures with B3LYP/6-311++G(d,p). All preparations for docking were carried out by with Discover Studio Visualizer 4.0 (DSV 4.0) software [56]. Then, active residues of the receptors were detected as ASP172, ASN168, GLN165, TYR129, ASP52, ASP48, ARG45, TYR41 and PHE22, according to these active region the grid parameters were determined as 62x60x60 $Å^3$ x, y, z dimesions, 0.375 Å space and 20.265, 51.849, 35.854 x, y, z centers. As a result, the molecular docking result were obtained and listed in Table 6. In the table, the inhibition constants between compound **2-4** and 2ZCQ were computed by Ki=exp(ΔG/RT) equation (ΔG, R and T are the docking binding energy, gas constant (1.9872036×10^{-3} kcal/mol) and room temperature (298.15 K), respectively and were given in the last line of Table 6.

Table 6. AutoDockVina results of the binding affinity and RMSD values of different poses in Antimicrobial/2ZCQ inhibitor of the title compounds.

Mode	Compound **2**			Compound **3**			Compound **4**		
	Affinity (kcal/mol)	rmsdl.b.	rmsdl.b.	Affinity (kcal/mol)	rmsdl.b.	rmsdl.b.	Affinity (kcal/mol)	rmsdl.b.	rmsdl.b.
1	-8.4	0.000	0.000	-7.6	0.000	0.000	-7.0	0.000	0.000
2	-8.2	1.529	2.532	-7.4	2.628	5.818	-6.7	1.321	5.775
3	-7.3	2.195	2.685	-7.2	5.038	7.559	-6.6	12.556	14.629
4	-7.0	4.038	5.947	-7.1	5.096	8.221	-6.5	1.318	2.237
5	-6.9	17.377	20.050	-7.1	5.873	10.118	-6.4	1.740	3.152
6	-6.7	4.238	6.175	-6.9	15.024	17.925	-6.4	13.353	15.270
7	-6.6	3.562	5.825	-6.9	2.474	5.937	-6.4	13.150	16.214
8	-6.6	6.381	11.895	-6.8	6.807	9.960	-6.2	2.006	6.086
9	-6.6	6.158	11.504	-6.7	5.764	8.453	-6.2	1.557	6.020
10	-6.6	17.111	18.717	-6.7	15.685	18.481	-6.1	3.121	7.217
Inhibition constant: 0.696234 μM Hydrogen bonding: 2				Inhibition constant: 2.68633 μM Hydrogen bonding: 0			Inhibition constant: 7.39542 μM Hydrogen bonding: 1		

Additionally, 3D (a) and 2D (b) molecular docking shapes of between compound **2-4** and 2ZCQ were depicted as in **Fig. 10-12**. From the docking scores (**Table 6**) according to the binding energies the best bindings were found between compound 2 and 2ZCQ protein with -8.4 kcal/mol energy, 0.696234 μM inhibition constant and two hydrogen bonding. Here active hydrogen bonding was observed between ARG45 residue and O17 atom with 3.10 Å. From **Fig. 10-12** the other interaction types and bonding lengths could be seen clearly. These outcomes concluded that the compounds **2-4** are potent inhibitor for PDB: 2ZCQ receptor.

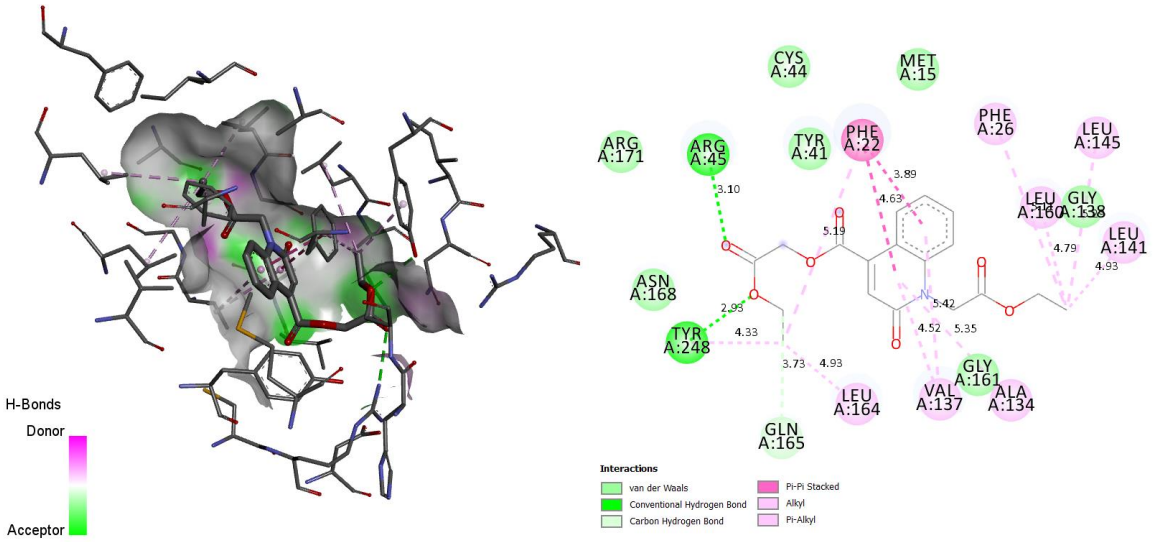

Fig. 10. (a) 3D and (b) 2D molecular docking results of the compound **2**+2ZCQ.

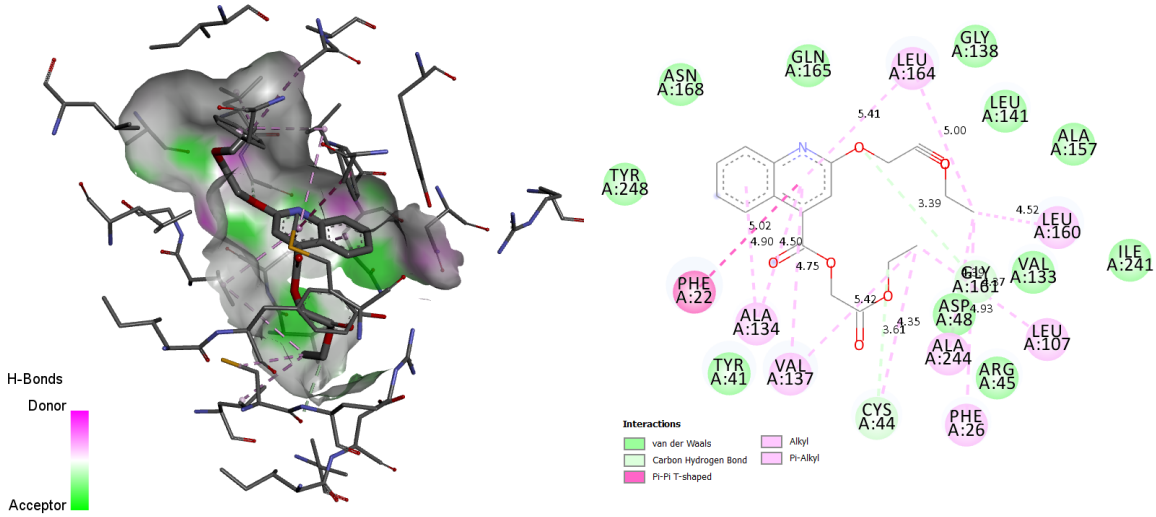

Fig. 11. (a) 3D and (b) 2D molecular docking results of the compound **3**+2ZCQ.

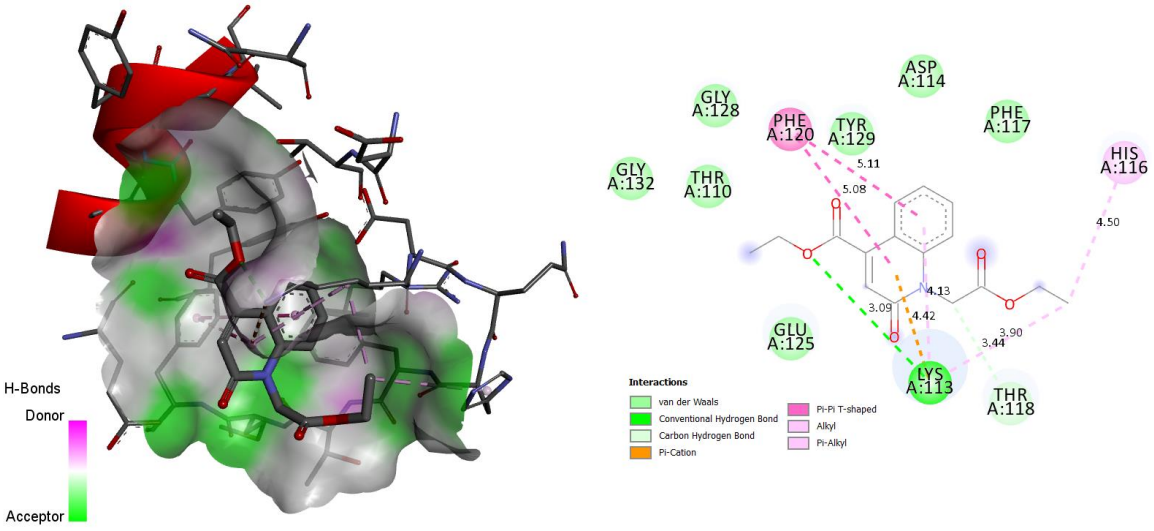

Fig. 12. (a) 3D and (b) 2D molecular docking results of the compound **4**+2ZCQ.

3.11. Drug-Likeness Study

Drug-Likeness properties of the compound **2-4** were studied in this part and the drug-likeness results were tabulated as in Table 7. These parameters were taken from SwissADME web page [57]. Because these parameters are very crucial in drug design and its potential to be a drug. According to the Lipinski rules, the candidate molecules must have 5 important properties in literature as follows [58]:

- MlogP ≤ 5
- Molecular weight (MW) ≤ 500 g/mol
- Number of H-bond acceptor (HBA) ≤ 10 and number of H-bond donors (HBD) ≤ 5
- Number of rotable bonds (n_{Rot}) ≤ 10
- Topological Polar Surface Area (TPSA)< 140 Å²

From the results, we can say that our compounds **2-4** are accordance with the criteria defined Lipinski rules above and there is no violations. Furthermore, the bioavailability radars and predicted Boiled-Egg plot were created by taking these rules into consideration and depicted **Fig. 13** and **14**, respectively.

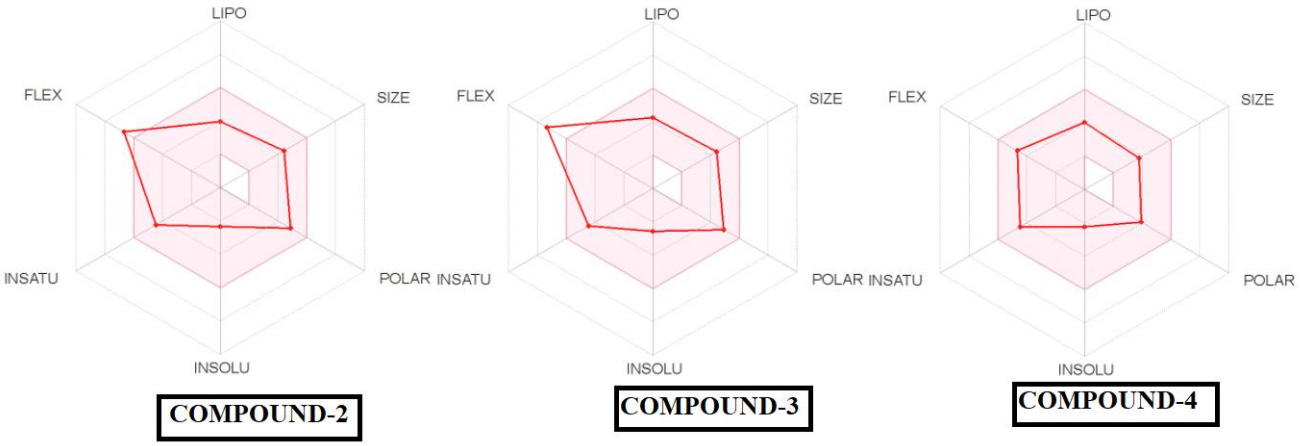

Fig. 13. The bio-availability radar of the title compounds.

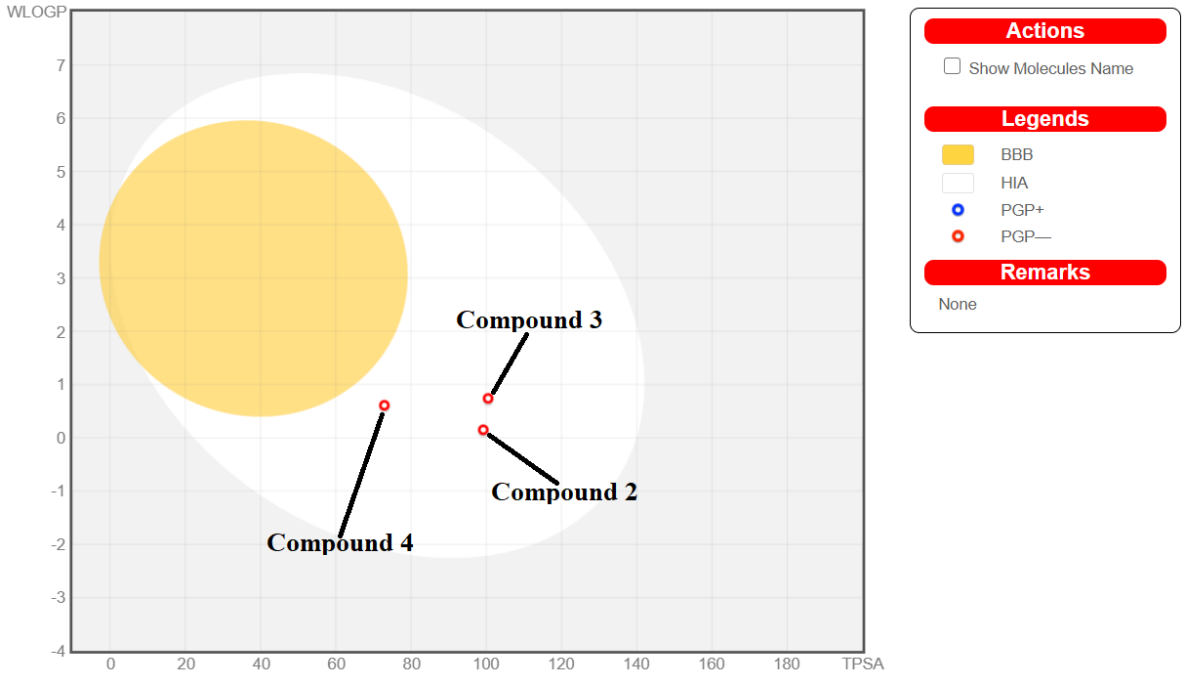

Fig. 14. The predicted Boiled-Egg plot of the title compounds.

Table 7. Drug-Likeness properties of the Ata-1-Ata-9 compounds.

Compound	MW	n_{Rot}	HBA	HBD	TPSA	M log *P*	Lipinski rule violation
2	363.36	10	7	0	99.21	0.81	0
3	363.36	11	8	0	100.49	1.21	0
4	305.33	7	5	0	72.91	1.18	0

Conclusions

In the present work, three new quinoline derivatives have been synthesized by alkylation of 2-oxo-1,2-dihydroquinoline-4-carboxylic acid with ethyl 2-bromoacetate, and characterized by FT-IR, ^{1}H-NMR, ^{13}C-NMR, single crystal X-ray diffraction (XRD). Comparisons between theoretical and experimental ^{1}H and ^{13}C NMR chemical shifts show good correlations among them. The Hirshfeld surface analysis of **3** and **4** shows that the most important contributions for the crystal packing are from H...H (46.1 and 47.1 %), O...H/H...O (32.1 and 29.4%) and C...H/H...C (14.6 and 18.2%) and interactions. In addition, compound **4** showed the most potent antibacterial activity against *S. aureus* with MIC value of 6.25 µg/mL. In addition, molecular docking results, we can say that the title compounds are potent inhibitor for 2ZCQ. Finally, drug-likeness studies showed that the title compounds have favourable pharmacological properties and their potentials as a drug is promising according to the traditional Pfizer five rules

Conflicts of interest

All authors declare that there are no conflicts of interest.

Acknowledgements

This work is supported by UM5R, we would like to acknowledge the UATRS-CNRST and Analysis and Characterization Platform ACP-FSR. The authors would like to thank Prof. Dr. Fatih Ucun for his helpful contribution and Gaussian Calculations. LVM thanks the Hercules Foundation for supporting the purchase of the diffractometer through project AKUL/09/0035.

Supporting Information Available: Figures S1-S13 and **Tables S1-S2**.

References

[1] J. Al Salman, L. Al Dabal, M. Bassetti, W. A. Alfouzan, M. Al Maslamani, B. Alraddadi, S. Kanj. Management of Infections Caused by WHO Critical Priority Gram-Negative Pathogens in Arab Countries of the Middle East: A Consensus Paper. Int. J. Antimicrob. Agents, (2020) 106104.

[2] N. B. Rajendran, N. T. Mutters, G. Marasca, M. Conti, F. Sifakis, C. Vuong. Mandatory surveillance and outbreaks reporting of the WHO priority pathogens for research & discovery of new antibiotics in European countries. Clin. Microbiol. Infect. *26*(7) (2020) 943-e1.

[3] X.M. Chu, C. Wang, W. Liu, L.L. Liang, K.K. Gong, C.Y. Zhao, K.L. Sun. Quinoline and quinolone dimers and their biological activities: an overview. Eur. J. Med. Chem. 161 (2019) 101-117.

[4] B. S. Matada, R. Pattanashettar, N. G. Yernale. A Comprehensive Review on the Biological Interest of Quinoline and its Derivatives. Bioorg. Med. Chem. (2020) 115973.

[5] A. Dorababu, Report on Recently (2017–20) Designed Quinoline-Based Human Cancer Cell Growth Inhibitors. ChemistrySelect, *5* (2020) 13902-13915.

[6] P. Yadav, K. Shah, Quinolines, a perpetual, multipurpose scaffold in medicinal chemistry. Bioorg. Chem. (2021) 104639.

[7] P. P. Thakare, A. D. Shinde, A. P. Chavan, N. V. Nyayanit, V. D. Bobade, P. C. Mhaske, Synthesis and Biological Evaluation of New 1, 2, 3-Triazolyl-Pyrazolyl-Quinoline Derivatives as Potential Antimicrobial Agents. ChemistrySelect, 5 (2020) 4722-4727.

[8] Z. Xu, C. Gao, Q. C. Ren, X. F. Song, L. S. Feng, Z. S. Lv. Recent advances of pyrazole-containing derivatives as anti-tubercular agents. Eur. J Med. Chem. 139 (2017) 429-440.

[9] A. Singh, M. Kalamuddin, M. Maqbool, A. Mohmmed, P. Malhotra, N. Hoda. Quinoline carboxamide core moiety-based compounds inhibit P. falciparum falcipain-2: Design, synthesis and antimalarial efficacy studies. Bioorg. Chem. (2020) 104514.

[10] R. D. Overacker, S. Banerjee, G. F. Neuhaus, S. M. Sephton, A. Herrmann, J. A. Strother, S. Loesgen, Biological evaluation of molecules of the azaBINOL class as

antiviral agents: Inhibition of HIV-1 RNase H activity by 7-isopropoxy-8-(naphth-1-yl) quinoline. Bioorg. Med. Chem. 27 (2019) 3595-3604.

[11] C. A. Costa, R. M. Lopes, L. S. Ferraz, G. N. Esteves, J. F. Di Iorio, A. A. Souza,. T. Rodrigues, Cytotoxicity of 4-substituted quinoline derivatives: Anticancer and antileishmanial potential. Bioorg. Med. Chem. 28 (2020) 115511.

[12] P. Panda, S. Chakroborty, Navigating the Synthesis of Quinoline Hybrid Molecules as Promising Anticancer Agents. ChemistrySelect, 5 (2020) 10187-10199.

[13] K. Douadi, S. Chafaa, T. Douadi, M. Al-Noaimi, I. Kaabi, Azoimine quinoline derivatives: Synthesis, classical and electrochemical evaluation of antioxidant, anti-inflammatory, antimicrobial activities and the DNA/BSA binding. J. Mol. Struct., 1217 (2020) 128305.

[14] A. R. Chabukswar, B. S. Kuchekar, S. C. Jagdale, P. D. Lokhande, V. V. Chabukswar, S. U. Shisodia, R. H. Mahabal, A. M. Londhe, N. S. Ojha. Synthesis and evaluation of analgesic, anti-asthmatic activity of (E)-1-(8-hydroxyquinolin-7-yl)-3-phenylprop-2-en-1 ones. Arabian J. Chem. 9 (2016) 704-712.

[15] J. Mo, H. Yang, T. Chen, Q. Li, H. Lin, F. Feng, W. Liud, W. Qu, Q. Guo, H. Chi, Y. Chen, Sun, H. Design, synthesis, biological evaluation, and molecular modeling studies of quinoline-ferulic acid hybrids as cholinesterase inhibitors. Bioorg. Chem. 93 (2019) 103310.

[16] T. A. Rano, E. Sieber-McMaster, P. D. Pelton, M. Yang, K. T. Demarest, G. H. Kuo. Design and synthesis of potent inhibitors of cholesteryl ester transfer protein (CETP) exploiting a 1, 2, 3, 4-tetrahydroquinoline platform. Bioorg. Med. Chem. Lett. 19 (2009) 2456-2460.

[17] M. H. El-Shershaby, K. M. El-Gamal, A. H. Bayoumi, K. El-Adl, H. E. Ahmed, H. S. Abulkhair, Synthesis, antimicrobial evaluation, DNA gyrase inhibition, and in silico pharmacokinetic studies of novel quinoline derivatives. Archiv Pharm., 354 (2021). 2000277.

[18] M. I. Ansari, S. A. Khan, Synthesis and antimicrobial activity of some novel quinoline-pyrazoline-based coumarinyl thiazole derivatives. Med. Chem. Res., 26 (2017).1481-1496.

[19] K. D. Katariya, S. R. Shah, D. Reddy, Anticancer, antimicrobial activities of quinoline based hydrazone analogues: synthesis, characterization and molecular docking. Bioorg. Chem., 94 (2020) 103406.

[20] N. C. Desai, A. Dodiya, N. Shihory, Synthesis and antimicrobial activity of novel quinazolinone–thiazolidine–quinoline compounds. J. Saudí Chem. Soci., 17 (2013) 259-267.

[21] X. Wenjie, L. Xueyao, M. Guixing, Z. Hongmin, C. Ya, K. Johannes, X. Jie, W. Song, N-thiadiazole4-hydroxy-2-quinolone-3-carboxamides bearing heteroaromatic rings as novel antibacterial agents: Design, synthesis, biological evaluation and target identification. Eur. J. Med. Chem., 188 (2020) 112022.

[22] V. G. Ugale, H. M. Patel, S. J. Surana. Molecular modeling studies of quinoline derivatives as VEGFR-2 tyrosine kinase inhibitors using pharmacophore based 3D QSAR and docking approach. Arabian J. Chem. 10 (2017) S1980-S2003.

[23] W. Al Garadi, Y. El Bakri, C. H. Lai, S. Karthikeyan, L. El Ghayati, J. T. Mague, E. M. Essassi, Synthesis, Crystal Structure and Computational Investigation of New 4-Phenyl-decahydro-1H-1, 5-benzodiazepin-2-one as Potent Inhibitor of Mu-opioid Receptor. ChemistrySelect, *5* (2020) 4601-4607.

[24] K. Karrouchi, S. A. Brandán, Y. Sert, H. El-marzouqi, S. Radi, M. Ferbinteanu, M. E. A. Faouzi, Y. Garcia, M. Ansar, (2020). Synthesis, X-ray structure, Vibrational spectroscopy, DFT investigation and biological evaluation studies of (*E*)-*N*′-(4-(dimethylamino)benzylidene)-5-methyl-1H-pyrazole-3-carbohydrazide, J. Mol. Struct. 1219, 128541.

[25] K. Karrouchi, S. A. Brandán, Y. Sert, M. El Karbane, S. Radi, M. Ferbinteanu, Y. Garcia, M. Ansar, (2020). Synthesis, structural, molecular docking and spectroscopic studies of (E)-N'-(4-methoxybenzylidene)-5-methyl-1H-pyrazole-3-carbohydrazide, J. Mol. Struct. 1225, 129072.

[26] B. Sureshkumar, Y. S. Mary, C. Y. Panicker, S. Suma, S. Armaković, S. J. Armaković, C.V. Alsenoy, B. Narayana. Quinoline derivatives as possible lead compounds for anti-malarial drugs: spectroscopic, DFT and MD study. Arabian J. Chem. 13 (2020) 632-648.

[27] Y. Bouzian, K. Karrouchi, Y. Sert, C. H. Lai, L. Mahi, N. H. Ahabchane, A. Talbaoui, J. T. Mague, E. M. Essassi, 2020. Synthesis, spectroscopic characterization, crystal

structure, DFT, molecular docking and in vitro antibacterial potential of novel quinoline derivatives. J. Mol. Struct. 1209, 127940.

[28] K. Chkirate, K. Karrouchi, N. Dege, N. K. Sebbar, A. Ejjoummany, S. Radi, N. N. Adarsh, A. Talbaoui, M. Ferbinteanu, E.M. Essassi, Y. Garcia, (2020). Co (ii) and Zn (ii) pyrazolyl-benzimidazole complexes with remarkable antibacterial activity. New J. Chem., 44, 2210-2221.

[29] K. Chkirate, S. Fettach, K. Karrouchi, N. K. Sebbar, E. M. Essassi, J. T. Mague, S. Radi, M. E. A. Faouzi, N.N. Adarsh, Y. Garcia, Novel Co (II) and Cu (II) coordination complexes constructed from pyrazole-acetamide: Effect of hydrogen bonding on the self assembly process and antioxidant activity. J. Inorg. Biochem. 191 (2019) 21-28.

[30] K. Chkirate, S. Fettach, M. El Hafi, K. Karrouchi, B. Elotmani, J. T. Mague, S. Radi, M. E. A. Faouzi, N.N. Adarsh, E. M. Essassi, Y. Garcia, Solvent induced supramolecular polymorphism in Cu (II) coordination complex built from 1, 2, 4-triazolo [1, 5-a] pyrimidine: Crystal structures and anti-oxidant activity. J. Inorg. Biochem., 208 (2020) 111092.

[31] Y. Bouzian, M. S. H. Faizi, J. T. Mague, B. E. Otmani, N. Dege, K. Karrouchi, E. M. Essassi. Crystal structure and DFT study of benzyl 1-benzyl-2-oxo-1, 2-dihydroquinoline-4-carboxylate. Acta Cryst E. 75(7) (2019) 980-983.

[32] Y. Bouzian, K. Karrouchi, E. H. Anouar, R. Bouhfid, S. Arshad, E. M. Essassi. Crystal structure, DFT study and Hirshfeld surface analysis of ethyl 6-chloro-2-ethoxyquinoline-4-carboxylate. Acta Cryst E. 75(6) (2019) 912-916.

[33] A.D. Becke, J. Chem. Phys. 98 (1993) 5648.

[34] M.J. Frisch, G. Trucks, H.B. Schlegel, G. Scuseria, M. Robb, J. Cheeseman, G. Scalmani, V. Barone, B. Mennucci, G. Petersson, Gaussian Inc. Wallingford CT 27 (2009) 34.

[35] R. Dennington, T. Keith, J. Millam, Semichem Inc.: Shawnee Mission, KS (2009).

[36] Y. Bouzian, F. Hlimi, M. El Hafi, B. Hni, E. M. Essassi, J. T. Mague, Ethyl 2-{[2-(2-ethoxy-2-oxoethoxy) quinolin-4-yl] carbonyloxy} acetate. *IUCrData*, 3(10) (2018) x181438.

[37] M. Turner, J. McKinnon, S. Wolff, D. Grimwood, P. Spackman, D. Jayatilaka, M. Spackman, University of Western Australia (2017).

[38] O. Trott, A.J. Olson, J. Computat. Chem. 31 (2010) 455.

[39] Rigaku OD (2018). *CrysAlis PRO*. Rigaku Oxford Diffraction, Yarnton, UK.

[40] O. V. Dolomanov, L. J. Bourhis, R. J. Gildea, J. A. K. Howard, H. Puschmann. J. Appl. Cryst. 42 (2015) 339–341.

[41] G. M. Sheldrick, SHELXT–Integrated space-group and crystal-structure determination, Acta Cryst. A71 (2015) 3–8.

[42] G. M. Sheldrick, Crystal structure refinement with SHELXL, Acta Cryst. C71 (2015) 3–8.

[43] A. Talbaoui, N. Jamaly, A. I. Idrissi, M. Bouksaim, S. Gmouh, M. El Moussaouiti, A. Benjouad, Y. Bakri, Chemical composition and antibacterial activity of essential oils from six Moroccan plants. J. Med. Plants. Res. 6 (2012) 4593-4600.

[44] F.L. Hirshfeld, Bonded-atom fragments for describing molecular charge densities, Theor. Chim. Acta, 44 (1977) 129.

[45] S. Dhibar, P. Yadav, T. Paul, K. Sarkar, A. P. Chattopadhyay, A. Krawczuk, B. Dey, A bio-relevant supramolecular Co (ii)-complex for selective fluorescence sensing of μM range inorganic As (iii) in aqueous medium and its intracellular tracking in bacterial systems. Dalton Trans. 48 (2019) 4362-4369.

[46] D. Ghosh, S. Dhibar, A. Dey, P. Manna, P. Mahata, B. Dey, A Cu (II)-Inorganic Co− Crystal as a Versatile Catalyst Towards 'Click'Chemistry for Synthesis of 1, 2, 3-triazoles and β-hydroxy-1, 2, 3-triazoles. ChemistrySelect, *5* (2020) 75-82.

[47] D. Dey, R. K. Mondal, S. Dhibar, C. H. Lin, D. Schollmeyer, D. Chopra, B. Dey, Insights into the supramolecular features in isopropylmalonic and n-butylmalonic acids: Inputs from PIXEL and Hirshfeld surface analysis. J. Mol. Struct., 1122 (2016) 29-36.

[48] R. K. Mondal, S. Dhibar, P. Mukherjee, A. P. Chattopadhyay, R. Saha, B. Dey, Selective picomolar level fluorometric sensing of the Cr (vi)-oxoanion in a water medium by a novel metal–organic complex. RSC adv. 6 (2016) 61966-61973.

[49] M.A. Spackman, D. Jayatilaka, Hirshfeld surface analysis, CrystEngComm 11 (2009) 19.

[50] P. Politzer, J.S. Murray, The fundamental nature and role of the electrostatic potential in atoms and molecules, Theor. Chem. Acc., 108 (2002) 134-142.

[51] J. D. Guzman, A. Wube, D. Evangelopoulos, A. Gupta, A. Hüfner, C. Basavannacharya, Bhakta, S. Interaction of N-methyl-2-alkenyl-4-quinolones with ATP-dependent MurE ligase of Mycobacterium tuberculosis: antibacterial activity, molecular docking and inhibition kinetics. J. Antimicrob. Chemother., 66 (2011) 1766-1772.

[52] A.K. Kahlon, S. Roy, A. Sharma, Molecular Docking Studies to Map the Binding Site of Squalene Synthase Inhibitors on Dehydrosqualene Synthase of Staphylococcus Aureus, J. Biomol. Struct. Dyn. 28 (2010) 201.

[53] C.T. Walsh, M.A. Fischbach, Inhibitors of Sterol Biosynthesis as Staphylococcus aureus Antibiotics, Angew Chem. Int. Ed. 47 (2008) 5700

[54] S. Banu, R. Bollu, M. Naseema, P.M. Gomedhika, L. Nagarapu, K. Sirisha, C.G. Kumar, S.K. Gundasw, A novel templates of piperazinyl-1, 2-dihydroquinoline-3-carboxylates: Synthesis, anti-microbial evaluation and molecular docking studies, Bioorg. Med. Chem. Lett. 28 (2018) 1166.

[55] https://www.rcsb.org/.

[56] http://www.3dsbiovia.com/.

[57] http://www.swissadme.ch/.

[58] C.A. Lipinski, F. Lombardo, B.W. Dominy, P.J. Feeney, Experimental and computational approaches to estimate solubility and permeability in drug discovery and development settings, Adv. Drug Deliv. Rev. 23 (1997) 3.

HIGHLIGHTS

- Three novel quinoline derivatives were synthesized and characterized by FT-IR, ^{1}H NMR, ^{13}C NMR and single-crystal XRD.
- DFT calculations were performed.
- Hirshfeld surfaces analysis was investigated.
- The title compounds were also evaluated *in vitro* for their antibacterial activities
- Molecular docking studies between the title molecules and 2ZCQ protein were performed.

Credit Author Statement

Younos Bouzian: Conceptualization, Methodology. **Yusuf Sert:** Theoretical Calculations, Original Draft, Writing - Review & Editing**. Khalid Karrouchi:** Investigation, Original Draft, Writing - Review & Editing. **Luc Van Meervelt:** X-ray data, Validation, Collected the data. **Karim Chkirate and Lhassane Mahi:** Formal analysis**. Ahmed Talbaoui:** Antibacterial activities. **El Mokhtar Essassi and Noureddine Hamou Ahabchane:** Supervision.

Declaration of interests

☒ The authors declare that they have no known competing financial interests or personal relationships that could have appeared to influence the work reported in this paper.

☐The authors declare the following financial interests/personal relationships which may be considered as potential competing interests: